Deposition of silicon oxide films on silicon using HelixJet – an atmospheric-pressure plasma jet process below 100 °C

Rebohle, L.; Quade, A.; Schumann, T.; Blaschke, D.; Hübner, R.; Heller, R.; Foest, R.; Schäfer, J.; Skorupa, W.;

Originally published:

April 2022

Thin Solid Films 753(2022), 139257

DOI: https://doi.org/10.1016/j.tsf.2022.139257

Perma-Link to Publication Repository of HZDR:

https://www.hzdr.de/publications/Publ-33040

Deposition of silicon oxide films on silicon using HelixJet – an atmospheric-pressure plasma jet process below 100 °C

L. Rebohle[1], A. Quade[2], T. Schumann[1], D. Blaschke[1], R. Hübner[1], R. Heller[1], R. Foest[2], J. Schäfer[2], W. Skorupa[1]

[1]Institute of Ion Beam Physics and Materials Research, Helmholtz-Zentrum Dresden-Rossendorf, Bautzner Landstrasse 400, 01328 Dresden, Germany

[2]Leibniz Institute for Plasma Science and Technology (INP), Felix-Hausdorff-Straße 2, 17489 Greifswald, Germany

Corresponding author: Lars Rebohle, Institute of Ion Beam Physics and Materials Research, Helmholtz Zentrum Dresden Rossendorf, Bautzner Landstraße 400, 01328 Dresden, Germany, Tel.: +49 351 2603368, E-mail address: l.rebohle@hzdr.de

Abstract

Silicon oxide films are widely applied for their superior dielectric, chemical and mechanic properties as well as for their resistance against reactive chemicals. Simultaneously, there is an increasing number of applications which demand a low deposition temperature. In this work, we compare the material properties of SiO_x layers deposited at ca. 70°C by atmospheric-pressure plasma jet deposition (PA) with those of SiO_2 layers thermally grown or deposited by plasma-enhanced chemical vapour deposition. The films were deposited on silicon wafers and analysed using different analysis techniques. According to cross-sectional transmission electron microscopy and high-frequency capacitance-voltage measurements, the interface between the PA oxide and the Si substrate is smooth with no apparent defects and displays an electrically active interface defect density between 3.5-8.0×10^{12} cm^{-2} directly after deposition and below

2.0×10^{12} cm^{-2} after furnace annealing. Right after deposition, the PA oxide contains carbon and hydrogen in a concentration of several at%, and the SiO_2 plasma polymer network comprises several active centres (residual charge, free radicals, non-saturated bonds). The most abundant configuration is the $Si(-O)_4$ tetrahedron, followed by $Si(-O)_3$ with similar intensity. This indicates that there are still dangling Si bonds or bonds terminated by hydroxyl or methyl groups. After furnace annealing, the formation of the SiO_2 network is completed and the optical and electrical properties of the PA oxide converge to that of thermal oxide.

Keywords: dielectric coating, insulation, corrosion protection, silicon oxide, atmospheric plasma source, thin films

1. Introduction

There is no doubt that the superior volume and interface-to-silicon properties of SiO_2 layers thermally grown at around 1000°C on single-crystalline silicon wafers revolutionised modern microelectronic technology dramatically. In the early seventies, the mastering of the electronic instability problems of this materials system [1] opened the door to advanced CMOS chip technology, allowing the development of computers, the world wide web, advanced chips for many purposes, etc. Meanwhile, starting with the transition to sub-0.1 µm CMOS technology after the year 2000, high-*k* dielectrics like HfO_2 have replaced silicon dioxide as a gate material although a residual amount of SiO bonds is still needed to reach lowest interface state densities [2, 3].

Nevertheless, it has always been a challenge to look for other techniques beyond thermal oxidation to produce thin silicon dioxide layers with comparable quality, not only by thermal growth but also by deposition techniques. This was demonstrated already in the seventies by the IBM group of Gaind et al. [4-6] using CVD (chemical vapour deposition) at atmospheric pressure in a SiH_4-CO_2-HCl-H_2 system at 1000°C. Further, low-pressure CVD growth techniques were also coming on stream [7].

Moreover, especially in the context of MOS-gates for compound semiconductor materials with lower melting points than Si as well as low-cost electronics approaches, the lowering of the processing temperature became an important issue. Among the many approaches, CVD methods were developed which could reach nearly the quality level of thermally grown oxide layers, both in the volume and at the SiO_2/semiconductor interface, using a process temperature range of 100 – 300 °C, e.g. for Ge, GaAs, InP [8]. More recently, the NAOS technology (nitric acid oxidation of silicon) was developed to form thin, highly reliable SiO_2 layers at temperatures of 120 °C for electronic applications like thin-film transistors (see [9] and ref's 15-21 therein). Finally, atomic layer deposition [10] and various

plasma deposition methods emerged which use more complex silanes [11-14] including octamethylcyclotetrasiloxane (OMCTS) [15, 16]. In these publications, the evaluation of electrical properties was missing except ref. [16], where the surface recombination velocity was studied.

Another challenge, useful for applications, is the laterally selective deposition of silicon oxide (SiO_x) layers. . In the framework of a project to form anticorrosive SiO_x layers on top of metallic sheets for pipe organs consisting of Pb/Sn- alloys or brass, a non-thermal reactive plasma jet (HelixJet) [17] was applied for plasma-enhanced CVD (PECVD) using a gas mixture of OMCTS and argon. Under these conditions, surface temperatures as low as about 70°C during deposition have been realised. In the course of our study, optimised SiO_x layers were also deposited on top of silicon wafers to investigate the layer properties at a well-defined system. Surprisingly, using cross-sectional transmission electron microscopy (TEM) we found a nearly perfect interface microstructure as well as electrical interface defect densities of 10^{12} cm^{-2} determined from the flat band voltage of capacitance-voltage analysis. In this paper, we analyse the chemistry of the silicon oxide films, their optical and electrical properties and compare them with films prepared using thermal oxidation and PECVD as reference processes. Post-deposition annealing treatments were performed by furnace annealing (FA).

2. Materials and Methods

The HelixJet is a cylindrical plasma source which allows the generation of a spatially homogeneous and stable plasma under atmospheric pressure within the tube volume. Thereby, a radio-frequency (RF) voltage at 27.12 MHz is capacitively coupled to double helix electrodes placed outside a quartz tube (∅ 9 mm). The HelixJet had been developed by J. Schäfer at INP and its specifications were reported recently [18]. For deposition of SiO_x films, the tube is fed by the working gas, in this case argon and a small admixture of organic vapour of

octamethylcyclotetrasiloxane (OMCTS). To allow for a programmed movement over the substrate, the HelixJet was mounted on a scanning system, originally designed for optical 3D surface profilometry. The operation conditions used in this study are listed in Table 1.

Silicon wafers (4 inch, (100)-oriented, p-type, 1-5 Ωcm) were used as substrates for the deposition of SiO_x. Just before deposition, all wafers were cleaned in H_2O_2/H_2SO_4 followed by a 20 s HF etch in order to remove native oxide. The working distance between the outlet of the HelixJet and the substrate surface was kept at 2 mm. The meandering trajectory with a step size of 2 mm was programmed for deposition across an area of 200 x 200 mm^2. The deposition was performed with a travel speed of 1 mms^{-1}. Thus, a conform coating of the whole area can be achieved. Samples made by this technique are labelled as PA (plasma at atmospheric pressure) in the following.

For comparison purposes, SiO_x films were prepared using thermal oxidation as well as PECVD. The thermal oxide was grown in a quartz tube furnace typical for microelectronic technology and was considered as a reference for high-quality layers with excellent electronic and optical properties. An oxidation temperature of 1050 °C and an HCl-based dry oxygen atmosphere were used for the oxidation process to produce layers of about 100 nm thickness. The oxidation process was finished in-situ with an anneal step in dry nitrogen at the oxidation temperature. PECVD was performed with a Plasmalab System 100 of Oxford Instruments using a deposition temperature of 350 °C, a gas mixture of SiH_4 and N_2O a pressure of 133 Pa, and a RF power of 20 W. Post-deposition annealing treatments were performed by FA using a conventional quartz tube furnace at a temperature of 1050 °C for 30 min in dry nitrogen atmosphere.

Film thickness and refraction index in the range of 1 and 4 eV were determined by a spectroscopic ellipsometry (SE) using a VASE Woollam with monochromator HS-190 and a Cauchy model for the SiO_x layers. The interface between the SiO_x layer and the Si substrate

was characterised by High-Resolution Transmission Electron Microscopy in cross-sectional mode (HRTEM, image-C_s-corrected Titan 80-300, FEI).

The chemical and elemental composition were analysed by X-ray Photoelectron Spectroscopy (XPS), Nuclear Reaction Analysis (NRA), and Rutherford Backscattering Spectrometry (RBS), respectively. XPS was provided by an Axis Supra DLD (Kratos Analytical) equipped with a monochromated Al-Kα (1486.6 eV) X-ray source. It has a maximum energy resolution of 0.45 eV (Ag 3d) and an optimum local resolution of 7 µm (Au lattice). Charge neutralisation as well as a pass energy of 160 eV and 80 eV were used for the acquisition of survey and single-element spectra, respectively. Data processing was carried out using the CasaXPS software (version 2.3.15, Casa Software Ltd., UK). Information depth and detection limit are about 10 nm and 0.1 to 1 at%, respectively. The spectra were charge-corrected by positioning the O 1s peak at 532.4 eV for oxygen atoms in siloxane environment [19]. After charge correction the Si 2p peaks were fitted including four components representing the $Si(-O)_x$ tetrahedral constitution ($1 \leq x \leq 4$), where $Si(-O)_4$ corresponds to inorganic SiO_2. [20]

For NRA, the resonant reaction ^{15}N (6.385 MeV) + $^{1}H \rightarrow {}^{12}C + {}^{4}He+\gamma$-rays (4.43 MeV) was exploited. The hydrogen depth profile was determined by gradually increasing the incident energy of ^{15}N ions and thus moving the resonance at 6.385 MeV progressively to larger depths. For RBS, the 2 MV van de Graaff-accelerator of the HZDR Ion Beam Centre using a primary beam of 1.7 MeV He-ions was applied. The backscattering angle and the solid angle of the silicon detector were 170° and 35 msr, respectively. The spectra were measured with a charge of 20 µC. The evaluation of the raw data and the determination of thickness and chemical composition were made with the SimNRA software.

The electrical properties as breakdown field strength, leakage current and effective interface charge Q_{eff} were determined by current-voltage and high-frequency capacitance-voltage measurements (HF-CV) using a Keithley 4200 device. For this purpose, aluminium

dots with a thickness of 150 nm and an area of 0.5 mm^2 were photolithographically produced on top of the oxide layers. The rear-side contacts of the samples were also made of an aluminium layer.

3. Results

The refraction index at 2 eV (620 nm) for different types of oxide and different post-annealing steps is shown in Fig. 1 The reference value for thermal silicon dioxide is about 1.457 (Woollam data base). The sample (PA) deposited by HelixJet exhibits a slightly smaller refractive index of about 1.44. However, annealing of the PA sample at 1050°C causes an increase of the refractive index up to 1.469 (PA+FA). Finally, this value is very close to that of the PECVD sample with a value of 1.466. On the other hand, the annealing of the PECVD sample reduces the refractive index to 1.461, which is finally equal to the experimental value of thermal oxide. Please note, that the variation of the data points in Fig. 1 for one type of oxide is due to the variation of individual samples with nominally equal deposition and annealing conditions.

The PA sample reveals a complex annealing behaviour. Here, the increase of refractive index can be explained by post-polymerisation and densification by annealing indicated by a significant reduction of the layer thickness by 23 % (Table 2). In contrast, the PECVD samples do not change their film thickness, and the small reduction of the refractive index can be explained, in combination with the decrease of the hydrogen content (Table 2), by the evaporation of low-molecular components.

Fig. 2 displays the Si/SiO_2 interface region between the monocrystalline Si and the amorphous silicon oxide for thermal oxide (a) and PA (b). For both samples, there are no structural defects at the interface, demonstrating the high quality of the deposition process, especially with respect to the low deposition temperature of about 70 °C in case of the PA oxide.

Fig. 3a shows the atomic concentration of Si, O, C, and N for the PA oxide on Si. The PA oxide still contains carbon in a concentration of 3 to 4 at%, and there is an excess of oxygen. Assuming that carbon can replace Si in the SiO_2 network, the element ratio Si/C:O is 1:2.17 (~8% excess to the stoichiometric ratio of 1:2). This is qualitatively confirmed by RBS measurements indicating an oxygen excess of about 7% for the PA oxide compared to thermal oxide. In general, an excess of oxygen minimises dangling Si bonds and the concentration of oxygen deficiency centres, which is beneficial for good electrical properties of both the volume and the interface. In accordance with this, the analysis of the Si-O binding efficiency related to the Si2p bonding (Figure 3b) shows clearly a dominance of the $Si(-O)_3$ and $Si(-O)_4$-binding tetrahedra. The low number of $Si(-O)_1$ and $Si(-O)_2$-bindings indicate that they play only a minor role for the microstructure of the material. However, the high concentration of $Si(-O)_3$-binding tetrahedra shows that the SiO_2 network has not yet fully formed, and that a significant number of Si bonds are still terminated by CH_3 and OH groups [21]. The apparent deficiency of oxygen in the tetrahedral bonding distribution and the excess of oxygen found in XPS suggest that a larger amount of oxygen is bound outside the SiO_2 network, probably in form of OH groups or O_2 molecules. An additional contribution could also come from Si vacancy defects like Si-O-O-Si peroxy bridge defect centres [22].

The hydrogen content in the first 20 nm of the SiO_2 layer as measured by NRA is shown in Fig. 4. It is clearly seen that the PA and PECVD oxides contain a significant amount of hydrogen. Low-molecular fragments of hydrogen or interstitial water can be eliminated by a thermal post-processing. In case of the PA sample, hydrogen was even outgassing from the layer during the NRA-measurement. After an initially high concentration (light blue), the hydrogen content dropped to a low saturation level the during measurement; the value indicated by the dark blue column is the average over the measurement time. In the case of the annealed PA sample, the hydrogen content is strongly reduced due to the thermal treatment. In the cases of PECVD+FA and thermal oxide, the hydrogen concentration is below the detection limit.

Figure 5 displays the current density as a function of the applied electric field in accumulation (negative bias at the gate). The film thickness as determined by SE was used to obtain the applied electric field across the SiO_x layer. The PA as well as the PECVD sample exhibit high currents already at low applied electric fields. In addition, the curves for the PA sample strongly vary between individual dots. After annealing of both the PA and the PECVD oxide, low leakage currents and a later onset of tunnel injection around 5.5 $MVcm^{-1}$ is observed, which is roughly 1 $MVcm^{-1}$ earlier than in the case of thermally grown oxide. The breakdown field strength is, except for PECVD+FA, in the range of 9-10 $MVcm^{-1}$.

In Table 2, the values of the effective interface charge as determined from HF-CV measurements are also presented. Thermally grown oxide shows the typical, excellent values below 10^{12} cm^{-2}. On the other hand, the values for the atmospheric CVD process (PA) are in the range of 3.5-8×10^{12} cm^{-2} directly after deposition at about 70 °C and below 2×10^{12} cm^{-2} after an additional furnace annealing step. This is accompanied by a general reduction of the variation between individual devices. The PECVD sample exhibits the highest values of about 1.5-1.7×10^{13} cm^{-2}. In combination with the HRTEM images in Fig. 2 it can be concluded, that the interface between PA oxide and Si substrate is of high quality, even if the SiO_2 network of the PA oxide has not yet fully formed.

4. Conclusions

We successfully deposited and characterised Si oxide at 70°C onto a Si substrate (PA oxide) with the HelixJet - a non-thermal reactive PECVD technique under atmospheric pressure. According to cross-sectional HRTEM and HF-CV measurements, the interface between the PA oxide and the Si substrate is smooth with no apparent defects and displays an electrically active defect density between 3.5-8.0×10^{12} cm^{-2} directly after deposition and below 2.0×10^{12} cm^{-2} after furnace annealing.

In addition, the present study provides a deeper insight into post-polymerisation effects in silicon oxide films after atmospheric-pressure plasma jet deposition using OMCTS and the HelixJet plasma source. Right after deposition, the oxide network contains several active centres (residual charges, free radicals, non-saturated bonds). Hence, pure silicon dioxide has not yet fully formed. XPS shows evidence of a larger fraction of $Si(-O)_3$-binding tetrahedra, indicating that a significant number of Si bonds are open or terminated by hydroxyl or methyl groups. The PA oxide also contains excess hydrogen, carbon, and oxygen, probably bounded in the form of water, hydrocarbons, and O_2 molecules. Finally, the SiO_2 network has a slightly less dense structure than that of thermal oxide as evidenced by the low index of refraction and the strong densification during annealing. We assume that the relatively high conductivity at lower electric fields is caused by open molecular structures and structural defects which disappear after post-polymerisation has finished.

The application of furnace annealing finalises the formation of the SiO_2 network, and the optical and electrical properties of the PA oxide converge to that of thermal oxide. The application of furnace annealing seems to contradict the idea of a low-temperature oxide at first glance, but the replacement of furnace annealing by ultra-short time annealing like flash lamp or laser annealing could be a promising alternative.

Acknowledgments

Support by Ilona Skorupa, Andrea Scholz, Romy Aniol, and by the Nanofabrication and TEM Facilities Rossendorf at IBC is gratefully acknowledged.

References

[1] B. E. Deal, The current understanding of charges in the thermally oxidized silicon structure, J. Electrochem. Soc. 121 (1974), 198C.

[2] G.D. Wilk, R.M. Wallace, J.M. Anthony, High-kappa gate dielectrics: Current status and materials properties considerations, Journal of Applied Physics 89 (2001), 5243.

[3] R.M. Wallace, G.D. Wilk, High-kappa dielectric materials for microelectronics, Critical Reviews in Solid State and Material Sciences 28, 4 (2003), 231.

[4] A.K. Gaind, G.K. Ackermann, V.J. Lucarini, R.L. Bratter, Preparation and Properties of SiO_2 Films from SiH_4-CO_2 –H_2, J. Electrochem. Soc. 123 (1976), 111.

[5] A. K. Gaind, , G.K. Ackermann, A. Nagarajan, R.L. Bratter, Preparation and Properties of CVD Oxides with Low Charge Levels from SiH_4-CO_2 -HCI-H_2 System, J. Electrochem. Soc. 123 (1976), 238.

[6] L.A. Kasprzak, A. K. Gaind, Near ideal Si-SiO_2 interfaces, Jpn. J. Appl. Phys. 19 (1980), 99.

[7] J. A. Amic, G.L. Schnable, J.L. Vossen, Deposition of dielectric films on semiconductor devices, Journal of Vacuum Science and Technology 14 (1977), 1053.

[8] B.R. Bennett, J.P. Lorenzo, K. Vaccaro, A. Davis, Low Temperature Pyrolytic Deposition of High Quality SiO_2, J. Electrochem. Soc. 134 (1987), 2517.

[9] K. Imamura, M. Takahashi, Asuha, Y. Hirayama, S. Imai, H. Kobayashi, Nitric acid oxidation of Si method at 120 °C: HNO3 concentration dependence, J. Appl. Phys. 107 (2010), 054503.

[10] J.W. Lim, S.J. Yun, J.H. Lee, Low-temperature growth of SiO_2 films by plasma-enhanced atomic layer deposition, ETRI Journal 27 (2005), 118.

[11] S.E. Babayan, J.Y. Jeong, A. Schutze, V.J. Tu, M. Moravej, G.S. Selwyn, R.F. Hicks, Deposition of silicon dioxide films with a non-equilibrium atmospheric-pressure plasma jet, Plasma Sources Sci. Technol. 10 (2001), 573.

[12] Y.Y. Wu, H. Sugimura, Y. Inoue, O. Takai, Preparation of hard and ultra water-repellent silicon oxide films by microwave plasma-enhanced CVD at low substrate temperatures, Thin Solid Films 435 (2003), 161.

[13] V. Raballand, J. Benedikt, A. von Keudel, Deposition of carbon-free silicon dioxide from pure hexamethyldisiloxane using an atmospheric microplasma jet, Appl. Phys. Lett. 92 (2008), 091502.

[14] Nguyen et al., Atmospheric Plasma-Enhanced Spatial Chemical Vapor Deposition of SiO2 Using Trivinylmethoxysilane and Oxygen Plasma, Chem. Mater. 32 (2020), 5153.

[15] Y. Qi, Z.G. Xiao, T.D. Mantei, Comparison of silicon dioxide layers grown from three polymethylsiloxane precursors in a high-density oxygen plasma, J. Vac. Sci. & Techn. A 21 (2003), 1064.

[16] B. Hoex, F.J.J. Peeters, M. Creatore, M.A. Blauw, W.M.M. Kessels, M.C.M. van de Sanden, High-rate plasma-deposited SiO2 films for surface passivation of crystalline silicon, J. Vac. Sci. & Techn. A 24 (2006), 1823.

[17] J. Schäfer, F. Sigeneger, R. Foest, D. Loffhagen, K.D. Weltmann, On a non-thermal atmospheric pressure plasma jet used for the deposition of silicon-organic films, Eur. Phys. J. D 72 (2018), 90.

[18] J. Schäfer, A. Quade, K.J. Abrams, F. Sigeneger, M.M. Becker, C. Majewski, C. Rodenburg, HelixJet: An innovative plasma source for next-generation generation additive manufacturing (3D printing), Plasma Processes Polym.17 (2020), e1900099.

[19] D.S. Wavhal, J.M. Zhang, M.L. Steen, E.R. Fisher, Investigation of gas phase species and deposition of SiO_2 Films from HMDSO/O-2 plasmas, Plasma Processes Polym. 3 (2006), 276.

[20] J. Schäfer, R. Foest, A. Quade, A. Ohl, K.D. Weltmann, Chemical Composition of SiO_x Films Deposited by an Atmospheric Pressure Plasma Jet (APPJ), Plasma Process Polym.6 (2009), S519.

[21] J. Schäfer, K. Fricke, F. Mika, Z. Pokorna, L. Zajickova, R. Foest, Liquid assisted plasma enhanced chemical vapour deposition with a non-thermal plasma jet at atmospheric pressure, Thin Solid Films 630 (2017), 71.

[22] D. Ricci, G. Pacchioni, M.A. Szymanski, A.L. Shluger, A.M. Stoneham, Modelling disorder in amorphous silica with embedded clusters: The peroxy bridge defect center, Phys. Rev. B 64 (2001), 224104.

Tables

Table 1. Operation settings of the plasma source.

Quantity	**Range**	**Setting in this study**
RF power (27.12 MHz)	30 – 100 W	70 W
Gas flow (Argon)	100 – 2000 sccm	1000 sccm
Precursor (OMCTS)	0 – 1 g/h	0.2 g/h
Scanning velocity	0 – 1 mm/s	1 mm/s

Table 2. Characteristic layer properties as determined from spectroscopic ellipsometry (thickness, refraction index), NRA (hydrogen content) and HF-CV measurements (Q_{eff}).

Sample name	**Fabrication mode**	**Thickness [nm]**	**Refractive index (SE)**	**Hydrogen content %**	**Q_{eff} [10^{12} cm^{-2}]**
Thermal oxide	Thermal oxidation (1050 °C, HCl-grown)	110	1.459	~ 0.1	0.5
PECVD	Plasma-enhanced CVD	88	1.466	7.8	15-17
PECVD +FA	PECVD + Furnace annealing (1050 °C, 30 min)	88	1.461	~ 0.1	6-7
PA	atmospheric-pressure plasma jet deposition	78	1.436-1.444	3.5	3.5-8
PA+FA	PA + Furnace annealing (1050 °C, 30 min)	60	1.469	0.5	1.9

List of figure captions

Fig. 1. Refractive index determined from SE data for different oxides.

Fig. 2. Cross-sectional HRTEM of the Si/SiO_x interface for thermal oxide (a) and PA (b).

Fig. 3. Atomic concentration of Si, O, C, and N (a) and tetrahedral bonding distribution (b) of PA oxide layers on Si as determined by XPS.

Fig. 4. Hydrogen content for different oxides as determined by NRA. In case of PA, the light blue column indicates the initial value during NRA measurement, whereas the dark blue column is the average over the measurement time.

Fig. 5. Current density as a function of the electric field for different oxides.

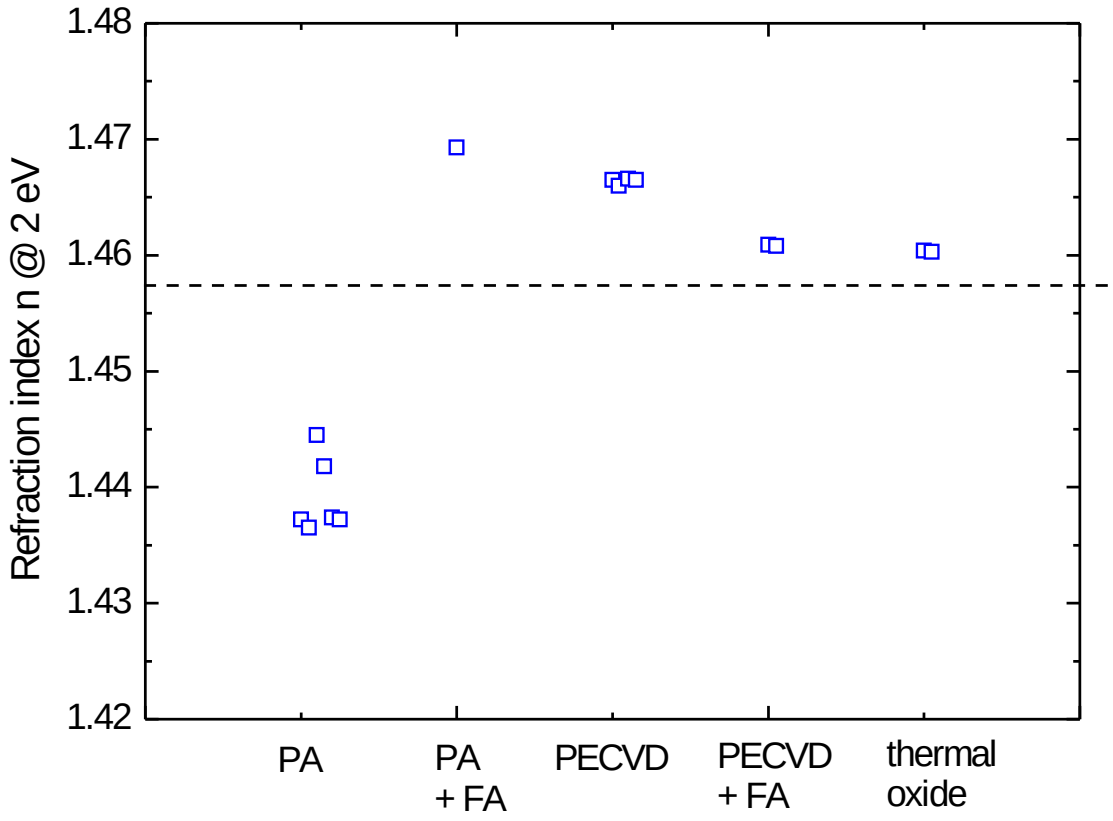
Refraction index n @ 2 eV
1.48
1.47
1.46
1.45
1.44
1.43
1.42
PA
PA
+ FA
PECVD
PECVD
+ FA
thermal
oxide

Fig. 1

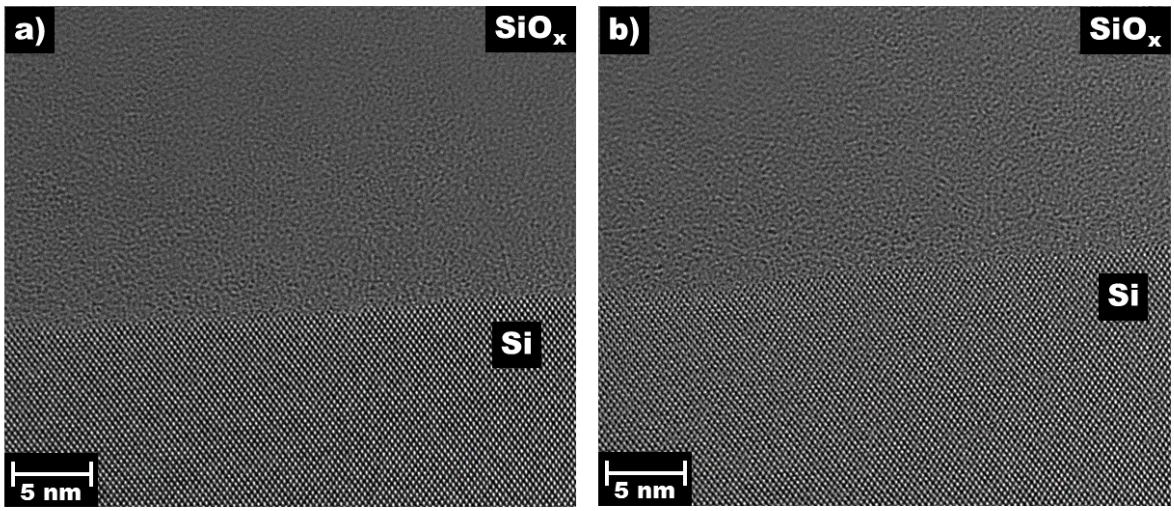

Fig. 2

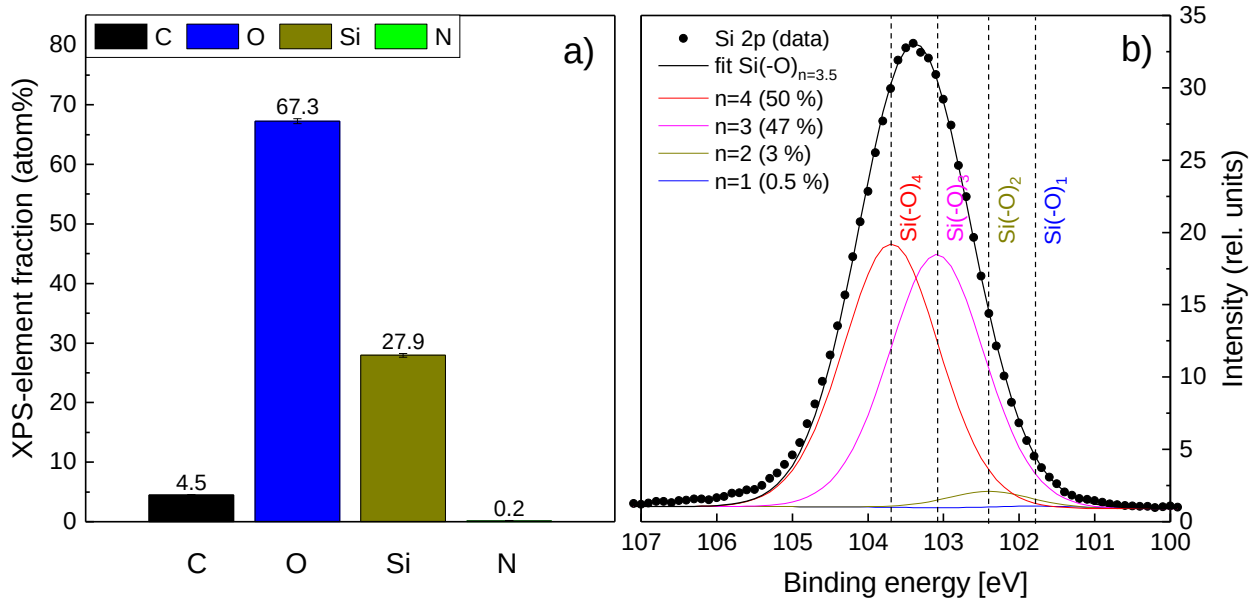
C
O
Si
N
a)
XPS-element fraction (atom%)
67.3
27.9
4.5
0.2
b)
Si 2p (data)
fit Si(-O)n=3.5
n=4 (50 %)
n=3 (47 %)
n=2 (3 %)
n=1 (0.5 %)
Si(-O)4
Si(-O)3
Si(-O)2
Si(-O)1
Intensity (rel. units)
Binding energy [eV]

Fig. 3

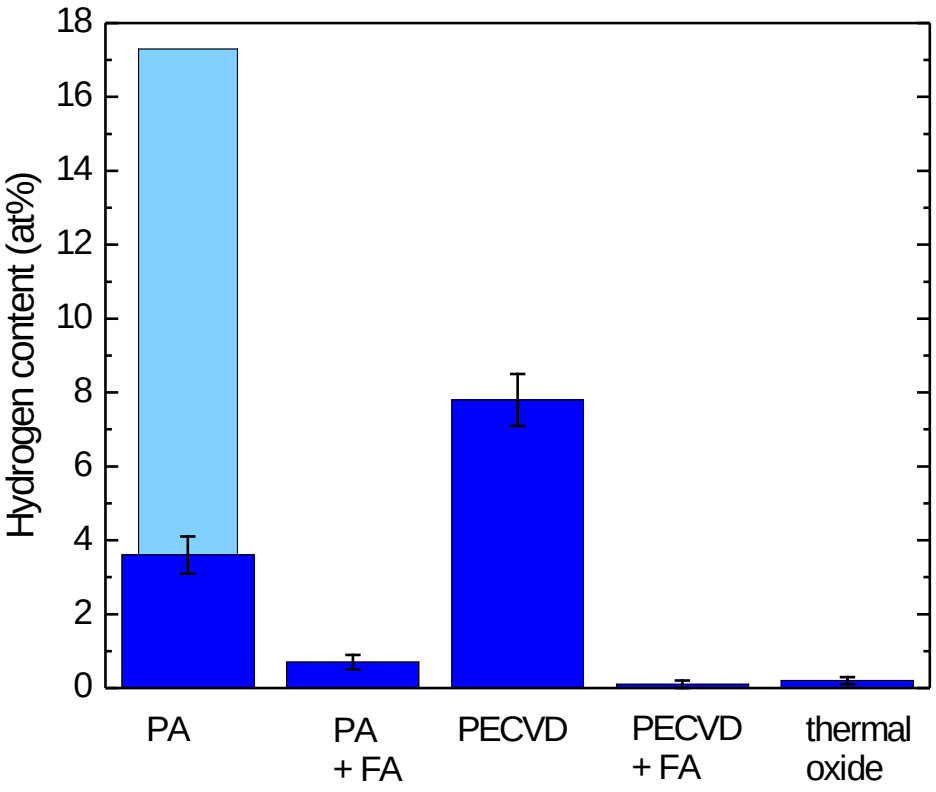
Hydrogen content (at%)
18
16
14
12
10
8
6
4
2
0
PA
PA
+ FA
PECVD
PECVD
+ FA
thermal
oxide

Fig. 4.

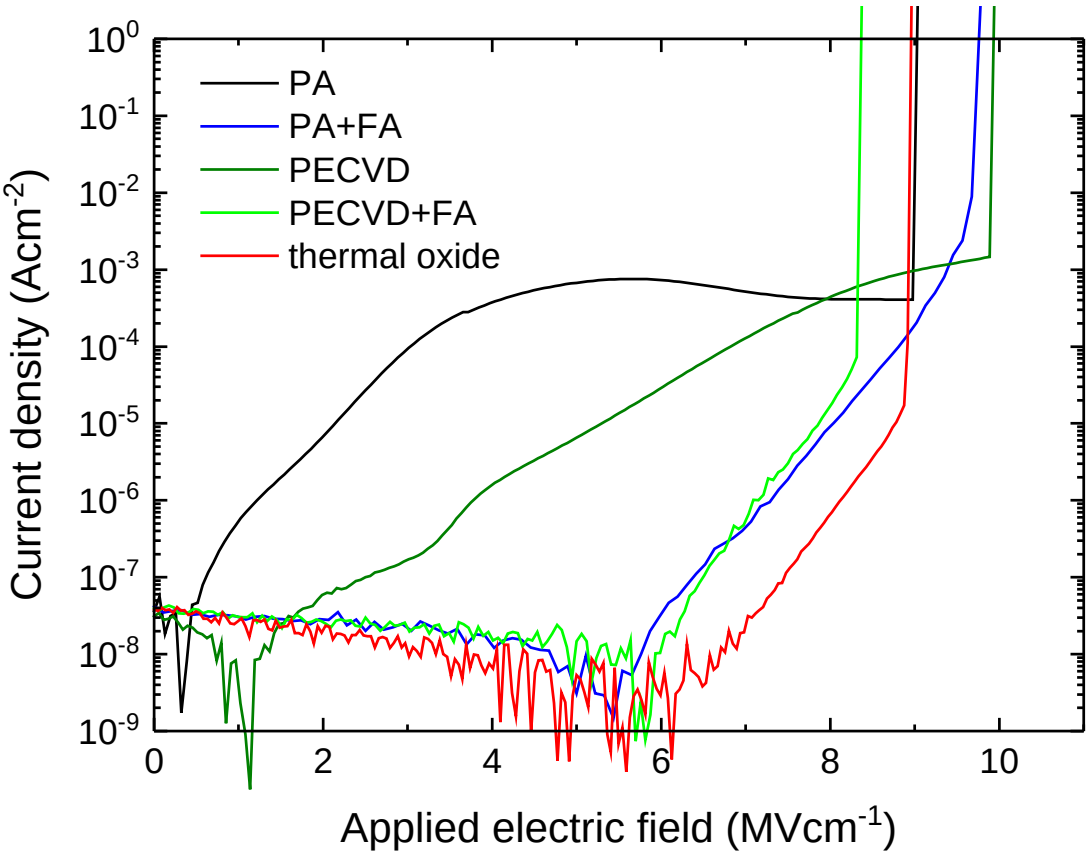
PA
PA+FA
PECVD
PECVD+FA
thermal oxide
Current density (Acm-2)
Applied electric field (MVcm-1)
10^0
10^-1
10^-2
10^-3
10^-4
10^-5
10^-6
10^-7
10^-8
10^-9
0
2
4
6
8
10

Fig. 5.